ICHEP94 Ref. gls0229
Submitted to Pa 01
Pl 02

DELPHI 94-61 PHYS 382
1st June, 1994

# Measurement of the $\Gamma_{b\bar{b}}/\Gamma_{had}$ Branching Ratio of the $Z$ by Double Hemisphere Tagging

DELPHI Collaboration

**Abstract**

Two measurements of $\Gamma_{b\bar{b}}/\Gamma_{had}$ are presented. Both measurements use about 250000 Z decays taken with the DELPHI detector in 1991 and rely mainly on the precision of the microvertex detector. One tagging method is as simple as possible so that background rates can reliably be predicted by Monte Carlo. The other one uses a more involved tagging technique and reduces the Monte Carlo dependence as much as possible. Combining both results, $\Gamma_{b\bar{b}}/\Gamma_{had}$ is found to be $0.2209 \pm 0.0041\,(stat.) \pm 0.0042\,(syst.) \pm 0.0018\,(\Gamma_{c\bar{c}})$.

# 1 Introduction

The ratio of the $b$ quark partial width of the $Z^0$ to its hadronic width is a particularly interesting quantity in the Standard Model. The propagator corrections that are measured with great precision elsewhere [1] largely cancel and only corrections to the $Zb\bar{b}$ vertex remain [2]. With a precise measurement of $R_b = \Gamma_{b\bar{b}}/\Gamma_{had}$ the top quark mass can be predicted essentially without residual model dependence.

In this paper we present two measurements with the DELPHI detector at LEP using about 250000 hadronic $Z^0$ decays taken in 1991.

Both measurements take advantage of the DELPHI microvertex detector which allows a highly efficient separation of $b$ and light quark events. The fraction of $b$ events and their tagging efficiency are measured in both cases simultaneously by comparing the numbers single and double hemisphere tagged events.

The first method which is similar to an analysis published by the ALEPH collaboration [3] uses only the significance of the impact parameters of charged tracks. Since this method is rather simple, the background from light quarks can be estimated reliably from a Monte Carlo simulation.

The second method is constructed to have reduced Monte Carlo dependence. As explained later this needs an extremely pure $b$ sample in the limit of very hard cuts. For this reason a more elaborate procedure combining event shape and microvertex variables in a multivariate analysis is used.

The outline of this paper is as follows. After a brief description of the DELPHI detector and the track and event selection, the main features of the two analysis are given. This is followed by a section explaining the combination of the two results and by our conclusions.

# 2 Track and Event Selection

The DELPHI detector has been described in detail elsewhere [4]. Therefore we shall mention here only the main features of the vertex detector (VD) which is essential to our analysis.

The vertex detector in the 1991 configuration was formed by 3 concentric shells of silicon strip detectors at radii of 6.5, 9 and 11 cm respectively. It covers the central region over a length of 24 cm and defined an angular acceptance of $27^0 - 153^0$, $37^0 - 143^0$ and $42^0 - 138^0$ for hits in one, two or three layers. Each layer was composed of 24 azimuthal modules with about 10% overlap in azimuth and each module consisted of 4 plaquettes along the beam direction. The intrinsic $r\phi$ resolution per layer, including alignment errors, has been evaluated to be $8\mu m$.

The track and event selection was slightly different in the two analysis, however the gross features are the same. Charged tracks were required to be well measured in the DELPHI tracking system. For the measurement of impact parameter related variables, they were only used if they had at least two hits in the VD. Neutral showers in the electromagnetic calorimeters were used to define hadronic Z decays and for the measurement of event shape variables. To select hadronic Z decays a minimum number of 5(6) charged tracks and 10(20) GeV of seen energy were required in first (second) analysis. To ensure that most tracks were well contained in the VD acceptance it was also required that the cosine of the polar angle of the thrust axis was smaller than 0.75.

# 3 Significance Analysis

This method is based on the fact that the $b$ and $\bar{b}$ quarks $Z^0$ from decays (and the corresponding heavy hadrons) are normally produced in opposite directions. On dividing such an event into 2 hemispheres (e.g. by the thrust axis), each will in general contain one $b$ hadron.

If with some tag one can select a pure $b$ flavour sample in one hemisphere, it is possible to find the efficiency of this selection and the fraction of $b\bar{b}$ events in the initial sample in a model-independent way by comparing the number of selected single hemispheres with the number of events in which both hemispheres are selected.

In practice the situation becomes more difficult because the background from the other flavours cannot be fully suppressed and thus should be subtracted properly. Additional problems arise from the fact that the hemispheres are not absolutely independent and the tag in one hemisphere biases the efficiency in the other, though this bias is small.

These statements may be expressed in the following form. If with some tag the efficiencies to select different flavours in one hemisphere are $\epsilon_b$, $\epsilon_c$ and $\epsilon_q$ (where $q$ stands for $(uds)$ quarks, which are not separated) and the efficiencies to select events in which both hemispheres are tagged are $\epsilon'_b$, $\epsilon'_c$ and $\epsilon'_q$, one can write:

$$\begin{aligned} R_H &= R_b \cdot \epsilon_b + R_c \cdot \epsilon_c + (1 - R_b - R_c) \cdot \epsilon_q \qquad (1) \\ R_E &= R_b \cdot \epsilon'_b + R_c \cdot \epsilon'_c + (1 - R_b - R_c) \cdot \epsilon'_q \\ &\simeq R_b \cdot \{\epsilon_b^2 + \rho_b \cdot (\epsilon_b - \epsilon_b^2)\} + R_c \cdot \epsilon_c^2 + (1 - R_b - R_c) \cdot \epsilon_q^2. \qquad (2) \end{aligned}$$

In these equations $R_H$ is the fraction of tagged hemispheres, $R_E$ the fraction of events in which both hemispheres are tagged and $R_b$ and $R_c$ the fractions of $Z^0 \to b\bar{b}$ and $Z^0 \to c\bar{c}$ events respectively in the initial sample. It is supposed that hadronic decays of the $Z^0$ consist of $b\bar{b}$, $c\bar{c}$ and light quark final states, so that the fraction of the light quarks may be written as $R_q \equiv (1 - R_b - R_c)$. The event efficiency for the $b$ flavour, $\epsilon'_b$, is expressed as $\epsilon'_b = \epsilon_b^2 + \rho_b \cdot (\epsilon_b - \epsilon_b^2)$, which takes into account the correlation between hemispheres $\rho_b$. This form comes from the definition of correlation $\rho = \frac{<(x-\mu_x)\cdot(y-\mu_y)>}{\sigma_x \cdot \sigma_y}$, which in the given case leads to $\rho_b = \frac{\epsilon'_b - \epsilon_b^2}{\epsilon_b \cdot (1-\epsilon_b)}$. For $c$ and $uds$ flavours the tag efficiencies $\epsilon_c$ and $\epsilon_q$ are small enough that the corresponding correlations do not influence $R_b$ and $\epsilon_b$ and thus are not included in the equations above.

From eqns. 1 and 2 one can extract the fraction $R_b$ and tagging efficiency $\epsilon_b$, provided the values $\epsilon_c$, $\epsilon_q$, $\rho_b$ and $R_c$ are known. The value of $R_c$ can be taken from the world average results [1], while $\epsilon_c$, $\epsilon_q$, $\rho_b$ are extracted from the Monte Carlo. If the $b$ purity of the tagged sample is high, the dependence on Monte Carlo is small and may be included in the systematic uncertainties. For the correct assignment of the errors to the measured values of $R_b$ and $\epsilon_b$, the correlation of the variables $R_H$ and $R_E$ which are not independent have been taken into account.

## 3.1 The Tagging Technique

For the tagging of $b$ flavour in hadronic decays of $Z^0$ we use the probability method, proposed originally in [3]. It is based on the fact that, because of the non-zero lifetime of hadrons with heavy flavour content, tracks of particles from decays of such hadrons have

large positive [1] impact parameter with respect to the primary vertex while tracks from the primary vertex have impact parameters which are smaller in absolute value and may be either positive or negative with the same frequency.

For the reconstruction of the primary vertex and in the following analysis, at least 3 tracks with more than one hit in the vertex detector were required. The primary vertex was reconstructed in every event using beam spot information as a constraint. The rms resolution of vertex reconstruction is around 50 $\mu$m for light quarks and 85 $\mu$m for the $b$ quark. The poorer resolution for the events with a $b$ quark is mainly due to the tracks from the secondary vertices which cannot be completely removed from the fit of the primary vertex.

The negative significance distribution, where the significance is defined as the impact parameter divided by its error, reflects mainly the detector resolution and is used to build the probability function $P(S_0)$, which is by definition the probability for tracks from the primary vertex to have an absolute significance $S_0$ or greater. Mathematically this function is obtained for negative values of significance by integration of the negative significance distribution over the range below $S_0$, and assuming that for positive significance $P(S_0)$ should be the same:

$$P(S_0) = \begin{cases} \int_{S<S_0} \rho(S) dS & \text{if } S_0 < 0 \\ P(-S_0) & \text{if } S_0 > 0, \end{cases} \tag{3}$$

where $\rho(S)$ is the probability density function of the significance distribution, which is also called the resolution curve. Additionally, to suppress tracks from the decays of $b$ hadrons which remain due to the wrong sign assignment to the impact parameters, for the construction of $\rho(S)$ only events which pass an anti $b$ cut $P_E^+ > 0.1$ are used. The definition of the variable $P_E^+$ will be given later. Here we just note that in the simulation this cut reduces the fraction of $b$ events in the sample to 6.5 %.

By definition, $P(S_0)$ has a flat distribution for tracks from the primary vertex, while for tracks from the secondary vertices the distribution peaks at low probabilities.

Using the probability function, which is calculated separately for tracks with 2 VD hits and more than 2 VD hits, one can compute the probabilities for all tracks in the event according to their values of significance. After that, for any group of $N$ tracks (which may be tracks from the total event or from one hemisphere) the $N$ track probability is defined as:

$$P_N \equiv \Pi \cdot \sum_{j=0}^{N-1} (-ln\Pi)^j / j!, \text{ where } \Pi \equiv \prod_{i=1}^{N} P(S_i). \tag{4}$$

This variable gives the probability for such a group of $N$ tracks with the observed values of significance to all be from the primary vertex. A group of tracks from the primary vertex should have a flat distribution of $P_N$, provided the significances of these tracks are uncorrelated. If the group includes tracks from secondary vertices, the distribution has a peak at low values of $P_N$. This is illustrated in fig. 1, where the distributions of $P_E^+$ for different flavours are shown. $P_E^+$ is computed using eqn. 4 for all tracks of the event with positive significance. As one can see, the distribution of $P_E^+$ for light quarks is approximately flat, while for $b$ quarks it has a sharp peak at 0.

[1] The sign of the impact parameter is defined with respect to the thrust axis. It is defined to be positive if the thrust axis is crossed in the direction of the track.

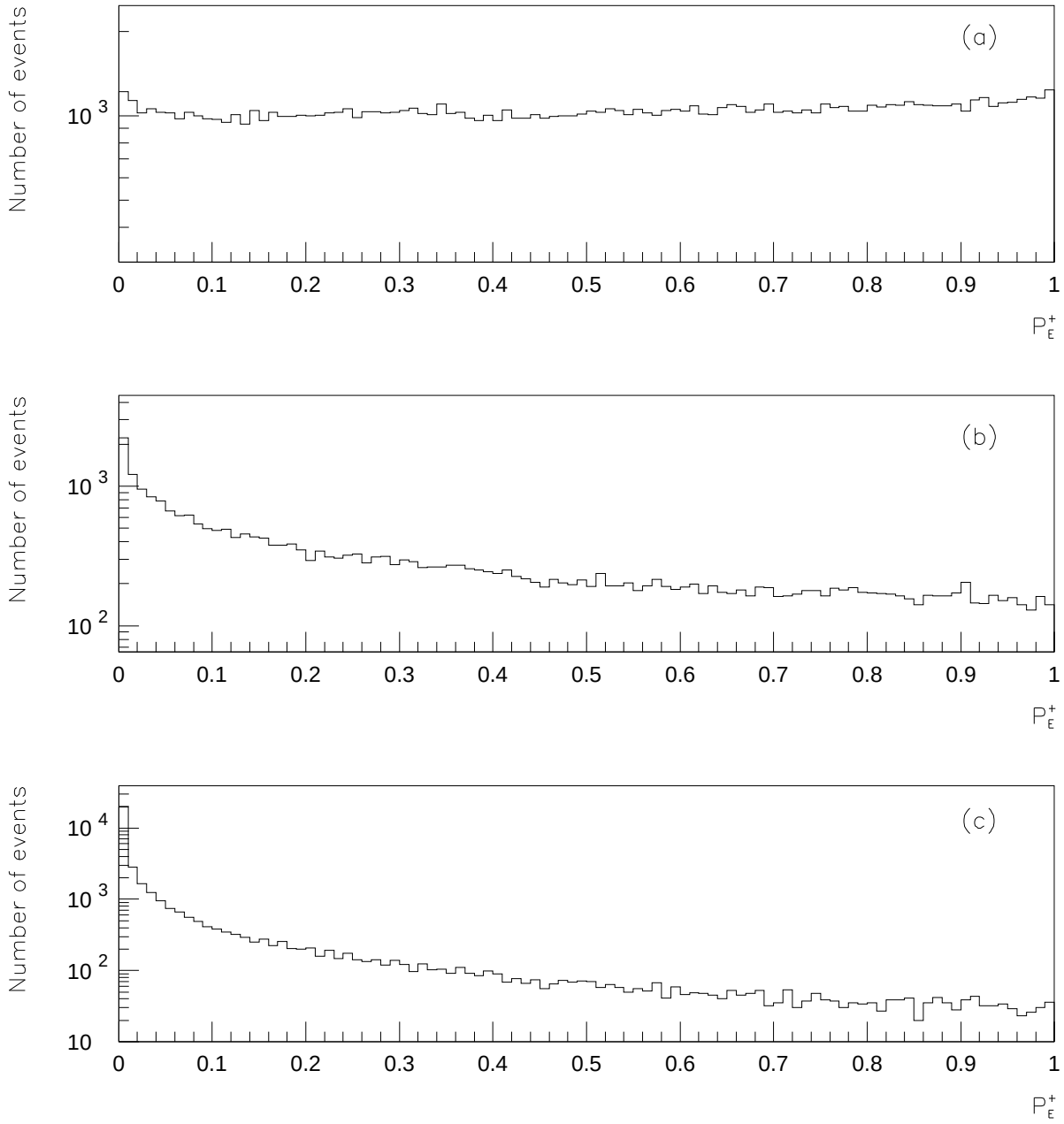


Figure 1: Distribution of event probability $P_E^+$ for tracks with positive impact parameters, for light quark events (a), charm quark events (b) and $b$-quark events(c) as obtained for MC.

The variable $P_E^+$ with the cut $P_E^+ > 0.1$ was used to obtain a $b$ reduced sample of events, which one needs to construct an undisturbed resolution curve. For the hemisphere tag another tagging variable, $P_H$, was used. $P_H$ is defined as the probability, computed using 4, for all tracks in one hemisphere, regardless of the sign of the impact parameter. It was found that this tagging variable gives almost the same efficiency for a given purity as the probability computed with only tracks of positive significance ($P_H^+$), but $P_H^+$ produces an additional correlation between hemispheres, because for the definition of the sign of impact parameter the common thrust axis was used. A cut of $\delta < 2.5$ mm was applied to reduce the background from $K^0$ and light hyperon decays. For the measurement of $R_b$ the selection cut $-\log(P_H) > 2.5$ was applied. This gives 89% purity of the tagging sample with a selection efficiency for $b$ flavour events of 23% (Monte Carlo estimates).

## 3.2 Determination of the Resolution Function

The resolution function plays a crucial role for the method of tagging and for correct determination of all values extracted from Monte Carlo. In this analysis the resolution function was determined using the data only and the Monte Carlo events were forced to have the same distribution as the data. This was achieved by the following steps.

- An analytical parameterization was found which describes the significance distribution with reasonable accuracy. It was checked not only for the spectrum integrated over all tracks, but also for subsamples with different momenta. All coefficients for it were extracted directly from a fit to the data.
- The errors both for data tracks and for simulated tracks were assigned in the same way depending on the track parameters.
- The simulated tracks were smeared around their "true" position (i.e. around the generated position of the parent vertex) according to the parameterization obtained.

This procedure should give the same distributions of significance for data and Monte Carlo, provided the distributions of the track parameters (momentum, polar angle etc...) are the same.

A comparison of the data and simulation resolution functions obtained by this technique is shown in fig. 2. Good agreement between data and Monte Carlo simulation was obtained practically over the whole range of significance values.

## 3.3 Estimates of Efficiencies and Correlations

For the measurement of $\Gamma_{b\bar{b}}$ , a cut $-\log_{10}(P_H) > 2.5$ was used. The values of $\epsilon_c$, $\epsilon_q$, $\rho_b$ with this cut were extracted from Monte Carlo simulation and the possible sources of uncertainties were included as systematic errors.

The value of $\epsilon_q$ was found to be:

$$\epsilon_q = (0.419 \pm 0.010(stat.) \pm 0.038(syst.)) \cdot 10^{-2}. \tag{5}$$

The first error in 5 comes from limited Monte Carlo statistics; the second is systematic. The different sources of systematic error are given in table 1. The systematic error due to uncertainties in the resolution function was estimated by varying the values of the

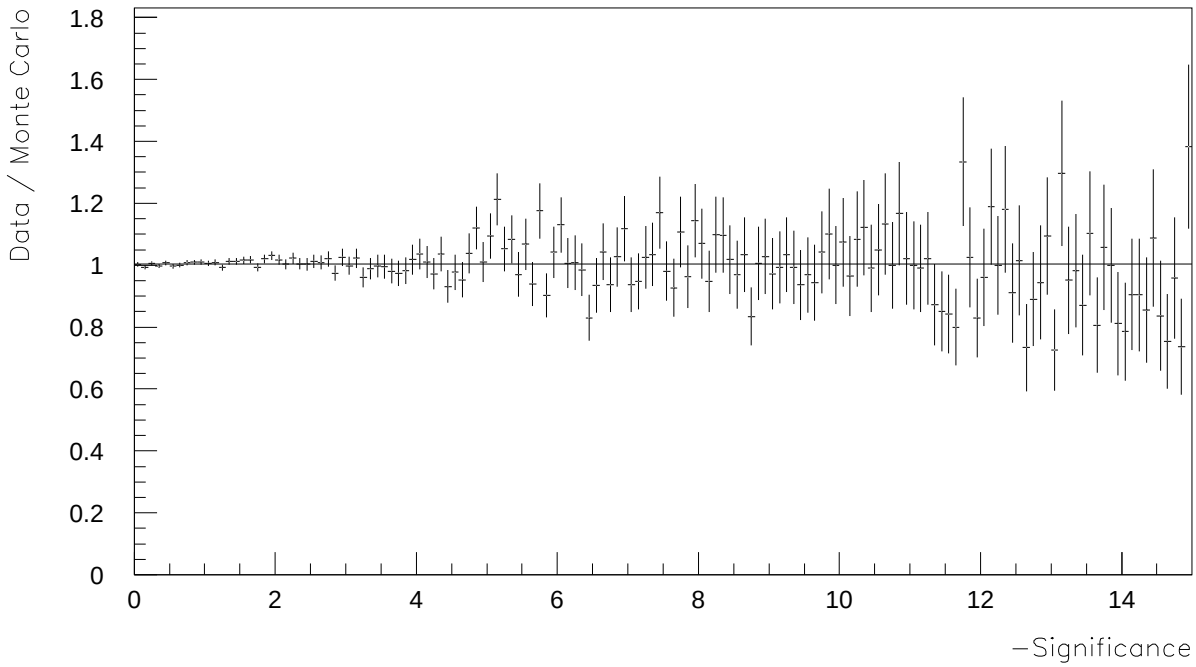


Figure 2: The ratio of significance distributions of Data and simulation for tracks with negative impact parameters

parameters used to describe the resolution within the error limits obtained from the fit of the resolution function.

Long-lived particles ($K^0$, $\Lambda$) and secondary interactions (including conversions of $\gamma \to e^+e^-$) are two of the main reasons for light quark background, responsible for about 40% of the total number of tagged light quark events. The systematic error from these sources was obtained supposing 20% uncertainty in the production rate of these long-lived particles (this number was obtained from the direct comparison of data and Monte Carlo).

The uncertainty from the difference in VD efficiencies between data and Monte Carlo was also included in the systematic error, though it is rather small.

| Source of systematics | $\Delta\epsilon_q \times 10^4$ |
|---|---|
| Resolution function | 1.74 |
| $K^0$, Hyperons, $\gamma \to e^+e^-$ | 3.40 |
| VD efficiency | 0.30 |
| Total | 3.83 |

Table 1: Systematic errors of light quark efficiency $\epsilon_q$

The efficiency to tag $Z^0 \to c\bar{c}$ was found to be:

$$\epsilon_c = (2.16 \pm 0.04(stat.) \pm 0.15(syst.)) \cdot 10^{-2}. \quad (6)$$

The sources of systematic error are listed in table 2. The resolution function contribution was estimated as for the light quark background. The efficiency of tagging $c$ quarks

depends on the relative production rate of $D^{\pm}$ and $D^0$ because the lifetimes of these two mesons differ. The relative production rate in $e^+e^-$ collisions was taken from data with $\sqrt{s}$ below the $b\bar{b}$ threshold [5], which excludes any contamination of $b$ flavour, and was varied by 20%. The part of the systematic error which comes from the charm hadron lifetime uncertainties was obtained by varying them within error limits taken from [5]. To estimate the uncertainty due to charm decay multiplicity, the values and errors of the average charge multiplicity for different mesons were taken from experimental measurements [6]. The uncertainty due to the fragmentation function is relatively small and was estimated by varying the mean energy of charmed mesons within error limits from [7].

| Source of systematics | $\Delta\epsilon_c \times 10^4$ |
|---|---|
| Resolution function | 7.2 |
| $D^{\pm}/D^0$ production rate | 8.4 |
| D lifetime | 7.0 |
| Charm decay Multiplicity | 6.5 |
| Fragmentation | 2.5 |
| Total | 14.8 |

Table 2: Systematic errors of charm quark efficiency $\epsilon_c$

The correlation between hemispheres occurs due to polar angle acceptance, to the fact that the beamspot constraint is common for both hemispheres, to the common primary vertex which was not so well reconstructed for events with long-lived $b$ hadrons and to hard gluon emission in Z decay which results in many-jet events and may boost $b$ hadrons into the same hemisphere.

The value of $\rho_b$ together with its systematic uncertainties was again determined from the Monte Carlo simulation:

$$\rho_b = (-0.13 \pm 0.37(stat.) \pm 0.18(syst.)) \cdot 10^{-2} \tag{7}$$

As one can see, the statistical error dominates in the determination of $\rho_b$. The systematic error includes the influence of the resolution function, the difference in the VD efficiency between data and Monte Carlo, a 10% change in the beamspot size (which corresponds to its stability and the accuracy of its determination) and a 6% variation of the errors of the primary vertex position (which corresponds to the maximal difference between data and Monte Carlo in the accuracy of primary vertex reconstruction for samples with different fractions of $b$ events). The change of the lifetime of $b$ hadrons may change the value of the correlation between hemispheres due to poorer primary vertex reconstruction and the systematic errors also include a contribution from varying the mean $b$ hadron lifetime within current world average value ($\tau_b = 1.521 \pm 0.034$ [8]). The systematic error from hard gluon emission, which may boost the two $b$ hadrons into the same hemisphere, is estimated to be 20% of the effect in the Monte Carlo. This number is deduced from the uncertainty in $\alpha_s$ and from the difference in the prediction of the Lund parton shower and matrix element model. In addition to these sources the cut on the thrust axis direction – $|cos\Theta_{thr}|$ – was varied from 0.65 to 0.85. With this variation the correlation factor $\rho_b$ (see eq. 7) did change from -0.4 to 2.4 % but the variation of $R_b$ is small (0.0007) and consistent with statistical fluctuations.

Table 3 shows the influence of the different sources of systematic error in the evaluation of $\rho_b$.

| Source of systematics | $\Delta\rho_b \times 10^4$ |
|---|---|
| Resolution function | 10.3 |
| Beam-spot size | 9.5 |
| Vertex-error estimate | 8.7 |
| VD efficiency | 2.4 |
| b-lifetime | 7.0 |
| Hard gluon emission | 1.3 |
| total | 18.1 |

Table 3: Systematic errors of correlation factor $\rho_b$

## 3.4 Results

For the measurement of $R_b$ the only remaining unknown parameter is $R_c$. It was taken from the value averaged over all LEP experiments [1]: $R_c = 0.171 \pm 0.014$. After the substitution of all values of efficiencies and correlation in eqns. 1 and 2 the following results were obtained:

$$\begin{aligned} \epsilon_b &= 0.2354 \pm 0.0043(stat.) \pm 0.0036(syst.) \\ R_b &= 0.2201 \pm 0.0040(stat.) \pm 0.0044(syst.) \pm 0.0019(\Gamma_{c\bar{c}}\ syst.). \end{aligned} \tag{8}$$

In eqn. 8 the systematic error coming from the value of $\Gamma_{c\bar{c}}$ is separated from all other sources. A change in the value of $R_c$ would change $R_b$: $\Delta R_b = -0.14 \times (R_c - 0.171)$.

The list of systematic uncertainties is given in table 6. It includes not only the errors discussed above from light and charm quark efficiencies and the correlation factor, but also the error due to a small bias towards $b\bar{b}$ events in the selection of hadronic Z decays.

The results in 8 were obtained for the probability cut $-\log_{10}(P_H) > 2.5$ which was selected to minimize the total error of $R_b$. The dependence of different error sources on the probability cut is shown in fig. 3. Figure 4 shows the variation of $R_b$ when changing the tagging cut. As one can see, there is no systematic dependence of the result on the value of the cut, but with variation of the cut the background content changes from 45% to 4% and the correlation factor changes from +1.5% to −0.5%. We consider this as a rigorous test of the procedure for the evaluation of efficiencies and correlations.

In the significance distribution there is an unavoidable contribution from the tracks from the decays of $b$ hadrons which changes the resolution curve and hence may change the final result. To check the influence of this effect on the obtained value of $R_b$, the cut on $P_E^+$, which was used to select the sample of events with reduced contents of $b$ hadrons, was varied from 0.05 to 0.50 and the complete analysis was repeated with the resolution functions determined with the different cuts on $P_E^+$. The variation of the cuts changes the content of $b$ flavour in the sample of events used for calibration from 12% to 3.5%, but the variation of $R_b$ is small (around 0.0013) and well within the expected uncertainty coming from the variation of the parameters of the resolution function.

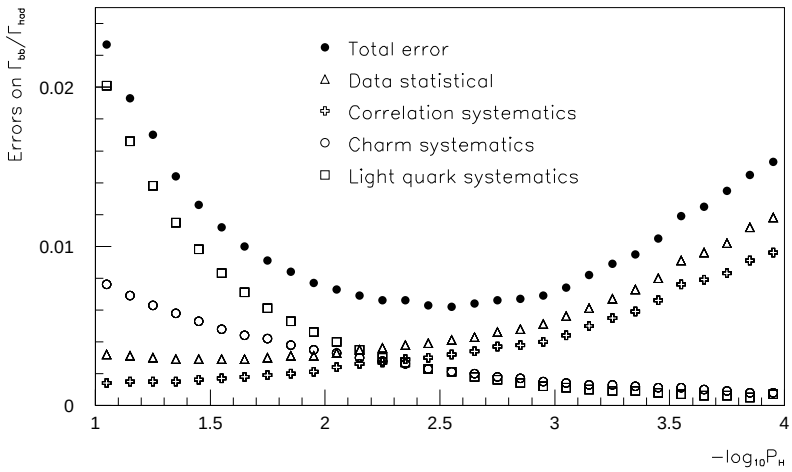


Figure 3: Errors of the measurement of $\Gamma_{b\bar{b}}\ /\Gamma_{had}$ as a function of the cut on $-\log_{10} P_H$.

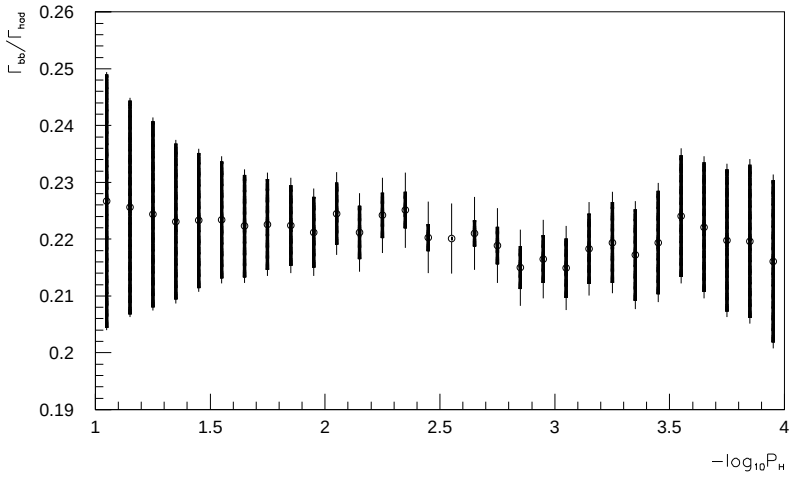


Figure 4: The value of $\Gamma_{b\bar{b}}\ /\Gamma_{had}$ as a function of the cut on $-\log_{10} P_H$ Both the total errors (narrow bars) and uncorrelated ones relative to the cut $-\log_{10} P_H > 2.5$ (wider bars) are shown.

In 1991 DELPHI took data at 7 different centre of mass energies around the $Z^0$ peak. The difference between the value of $R_b$ for different energies of the colliding beams and its value at the $Z^0$ peak (91.2 GeV) has also been measured. This difference is not sensitive to any of the systematic effects mentioned above and the precision of the estimate depends only on the available statistics. The small changes in efficiencies for different centre-of-mass energies were taken from the Monte Carlo. The results obtained are shown in fig. 5 and in table 4. The theoretical expectation of $\Delta R_b$ was calculated using the program ZFITTER [9]. As one can see, the results are consistent with the Standard Model prediction.

| Energy (GeV) | 88.5 | 89.5 | 90.2 | 92.1 | 93.1 | 93.7 |
|---|---|---|---|---|---|---|
| $R_b(E) - R_b(91.2\ \text{GeV}) \times 10^2$ | -2.69 | 0.31 | -0.62 | -0.17 | -0.37 | -0.78 |
| Error ($\times 10^2$) | 1.33 | 1.33 | 0.81 | 0.60 | 0.93 | 0.97 |

Table 4: The difference $R_b(E) - R_b(91.2\ \text{GeV})$ for the significance analysis

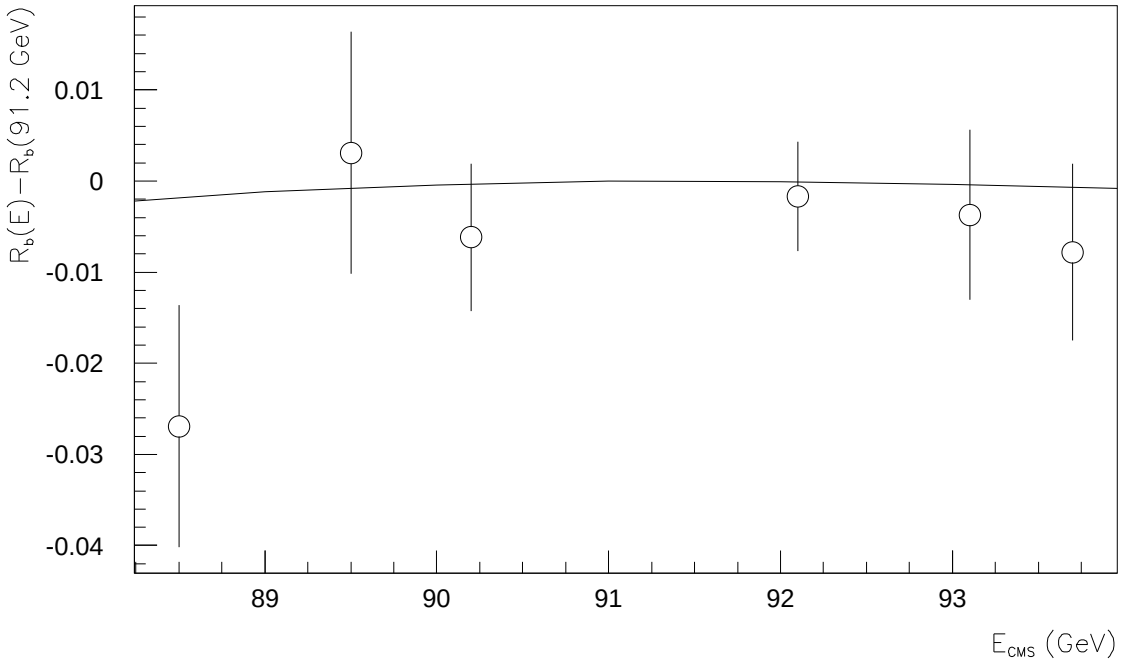


Figure 5: The difference $\Gamma_{b\bar{b}}$ /$\Gamma_{had}(E_{CMS})$-$\Gamma_{b\bar{b}}$ /$\Gamma_{had}(E_{CMS} = 91.2\ \text{GeV})$. The Standard Model prediction is shown by the solid line.

# 4 Multivariate Analysis

This analysis is optimized to reduce as much as possible the Monte Carlo dependence. A more detailed description of the method including some variants of the method presented can be found in [10].

## 4.1 Principle of the method

In this analysis the hadronic hemispheres are classified into three "flavours": $uds$, $c$ and $b$. The $u$, $d$ and $s$ flavours were merged in a single $uds$ light "flavour", since information on strange hadrons was not available and the tagging variables have very similar distributions for the three flavours.

### 4.1.1 Compositions and Classification Matrix

The aim of the tagging algorithm is to classify hadronic events into $N_T$ tags or categories, where $N_T$ is greater than the number $N_F$ of separated flavours. Let $C_I^l$ be the tagging probability of an event of flavour $l$ into the category $I$ ($I = 1, ..., N_T$ and $l = 1, ..., N_F$). The two dimensional array, $C_I^l$ (hereafter called *classification matrix* $\tilde{C}$) is the same for both hemispheres. Except for very hard gluon emission, the quark and the antiquark are produced in opposite hemispheres; [2], therefore the same flavour should appear in both hemispheres.

The tensor of the observables $D_{IJ}, (I, J = 1, ..., N_T)$, is defined as the fraction of events tagged as I and J for hemispheres 1 and 2 respectively. It is multinomially distributed. If the hemispheres are independent, the expected fraction of events $T_{IJ}$ can be written as

$$T_{IJ} = \sum_l C_I^l C_J^l R_l \qquad (I, J = 1, ..., N_T) \tag{9}$$

where $R_l$ is the flavour fraction for a given sample. $R_b$ is the branching ratio we want to extract.

The minimization of the objective function $G(C, x)$, defined as

$$G(C, x) = \sum_{IJ} \sum_{I'J'} (D_{IJ} - T_{IJ}) V^{-1} (D_{I'J'} - T_{I'J'}) \tag{10}$$

where $V$ is the covariance matrix of the $D_{IJ}$ elements, allows us to determine simultaneously the classification matrix $\tilde{C}$ and the composition of $R_l$.

The fit solution has to be compatible with the constraints: $\sum_l R_l = 1$, $\sum_I C_I^l = 1$ for all values of $l$. A method of Lagrange multipliers is appropriate to deal with this problem [11]. The tensor itself has to obey the normalization condition $\sum_{IJ} D_{IJ} = 1$ with the optional requirement of symmetry $D_{IJ} = D_{JI}$.

$V$ is a singular matrix due to the normalization condition. However, if one of the $D_{IJ}$ elements is excluded, a new diagonal covariance matrix $V^*$ can be defined [12] and the objective function is reformulated as

$$G(C, x) = \sum_{IJ} \frac{(D_{IJ} - T_{IJ})^2}{\sigma_{IJ}^2} \tag{11}$$

where the $D_{IJ}$ elements are now considered independent with Poissonian errors, $\sigma_{IJ}$.

The problem cannot be solved if the number of observables ($N_o$) is less than the number of unknowns ($N_u$). We have for a given $N_F$ and $N_T$, $N_o = N_T(N_T + 1)/2 - 1$, $N_u = N_T N_F - 1$. For example, for $N_F = 3$, $N_T$ must be at least 6.

[2] According to simulation, the fraction of $b\bar{b}$ pairs produced in the same hemisphere is 0.02.

### 4.1.2 The Rotation Degeneracy

The solution of the above described fit is not uniquely defined since there is a degeneracy inherent in the tensor parameterization. Let us introduce the set of vectors $\vec{V}_I$ whose three components are $(C_I^{uds}\sqrt{R_{uds}}, C_I^c\sqrt{R_c}, C_I^b\sqrt{R_b})$. Each tensor element $T_{IJ}$ can be expressed as the scalar product $T_{IJ} = \vec{V}_I \cdot \vec{V}_J$. The scalar product is invariant under rotations in the space where the vectors are defined. The vector $\vec{U}$ defined as

$$\vec{U} = \sum_I \vec{V}_I = (\sqrt{R_{uds}}, \sqrt{R_c}, \sqrt{R_b}) \tag{12}$$

can be interpreted as a composition vector of unit length. $\vec{U}$ and the set of $\vec{V}_I$ can be viewed as a rigid body. Once a particular solution has been found, other solutions may be generated by moving this rigid body according to three degrees of freedom; two degrees of freedom could be the position of the extremity of $\vec{U}$ on a sphere of unit radius, the third one an internal rotation around the $\vec{U}$ axis.

The degeneracy is removed in the $b$ sector if two or more estimates of the $C_I^b$ elements (hereafter denoted by $X_I^b$) are found. Let us define a modified objective function $G'(C, x)$ in which the estimates $X_I^b$ are introduced

$$G'(C, x) = G(C, x) \; + \; \sum_I \frac{(C_I^b - X_I^b)^2}{\sigma_I^2} \tag{13}$$

where $C_I^b$ are the same $\tilde{C}$ matrix elements as in function $G(C, x)$ and $I$ only runs over the $X_I^b$ considered. The $\sigma_I$ are errors on the $X_I^b$ estimates. The remaining degeneracy in the other sector can be removed, for instance, by fixing the $R_c$ to the Standard Model value. This constraint has no effect on any parameter of the $b$ sector.

## 4.2 Hemisphere Tagging

The tagging algorithm can be viewed as a technique to distribute the events with different flavours in a set of hemisphere categories. Multidimensional analysis has been chosen to provide a more efficient separation than a cumulative set of cuts. The details of the technique can be found in [13] and [14].

### 4.2.1 Vertex Reconstruction of Hemispheres

Each event is subdivided into two hemispheres according to the sphericity axis. The particles are grouped in jets using the LUND algorithm (LUCLUS) with $d_{join} = 2.5$ GeV and the jet direction is given by the internal thrust axis. All particles assigned to jets making an angle of less than $90^0$ with the sphericity axis are attributed to hemisphere one, the other ones to hemisphere two. In order to decrease correlations between opposite hemispheres, a primary vertex is computed on each side with an iterative procedure which includes all the charged particles of the hemisphere. If the fit probability of the global $\chi^2$ is less than 0.05 the particle which contributes with the largest value to the $\chi^2$ is removed, and a new vertex fit is attempted. The process continues until a probability greater than 0.05 is obtained or only two particles remain.

The beam spot position and dimensions were measured fill-by-fill. This information has been used as a constraint in the vertex fit on both sides. The beam spot size in

$x$ was around $150\mu m$ [3]. In $y$ it was less than $50\mu m$. The inclusion of this constraint increases the discriminating power of the tagging, but it represents a common feature of the hemispheres. However, the inclusion of the beam spot constraint does not seriously spoil the decorrelation of hemispheres.

### 4.2.2 Description of the Variables and Tags

The multidimensional analysis is based on a set of 12 discriminant variables per hemisphere. One variable ( boosted sphericity) is computed with momenta only, the remainder use the reconstructed particle trajectories near the interaction point. Three of them are connected to the $\chi^2$ fit of vertices associated with various sets of particles. Three are distances between "candidate secondary vertices" and the primary vertex, and are sensitive to decay lengths. Three variables are different counters of secondary particles, and finally two variables are estimates of the total energy and $P_t^2$ associated with secondary particles. A full description of these cuts and variables can be found in [14].

The probabilities $p_{uds}$, $p_c$ and $p_b$ to observe the 12 values of the variables for each hemisphere of an event are computed from model distributions taken from simulation. The logarithm of these three probabilities, called hereafter *"class-likelihoods"* ($L_{uds} = \ln\ p_{uds}$, $L_c = \ln\ p_c$ and $L_b = \ln\ p_b$), are the basis of our classification.

The hemispheres are first classified by 3 tags as follows. The flavour likelihoods are sorted in decreasing order as $L_{first}$, $L_{second}$, $L_{third}$. The hemisphere is tagged $uds$, $c$ or $b$ according to the highest probability, $L_{first}$. In order to define the six categories mentioned in section 4.1.1, we introduce a "winning margin"

$$\Delta = ln(p_{first}/p_{second}) \ = \ L_{first} - L_{second} \tag{14}$$

which is a sensitive indicator of tag clarity. Figure 6 represents the distributions of the "winning margin" observed in the simulation for the three tags.

The $uds$ and $b$ tags are afterwards subdivided into categories according with the following criteria:

- $uds - tight : \Delta > \Delta_{uds}^{cut}$ (category 1)
- $uds - loose : \Delta < \Delta_{uds}^{cut}$ (category 2)
- $b - loose : \Delta < \Delta_b^{cut,low}$ (category 4)
- $b - medium : \Delta_b^{cut,low} < \Delta < \Delta_b^{cut,high}$ (category 5)
- $b - tight : \Delta > \Delta_b^{cut,high}$ (category 6)

The values of the cuts are $\Delta_{uds}^{cut} = 2.0$, $\Delta_b^{cut,low} = 3.0$ and $\Delta_b^{cut,high} = 6.0$. They are chosen in order to have similar population in the categories. As can be seen in fig. 6, the $c$-tag (category 3) is less populated and poorly enriched. It has not been subdivided.

[3] However, a size of 200 $\mu m$ on average was introduced as a constraint in the fit.

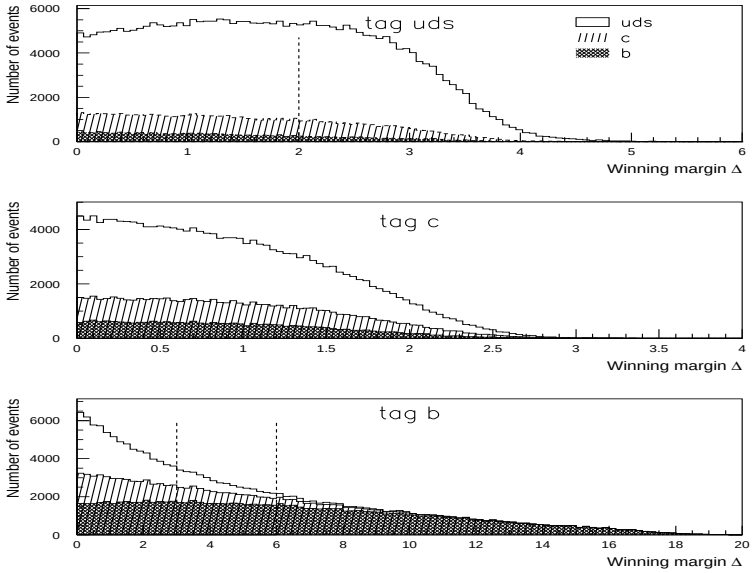


Figure 6: Distributions obtained from a Monte Carlo simulation of the winning margin $\Delta$ in the *uds*, *c* and *b* hemisphere tag. Each filled area style shows the different flavour contributions to the events in a given tag. The dashed lines show the cuts to separate the 6 different categories.

### 4.2.3 Simulation Results

This overview of the tagging performances - estimated from the simulated data set - is necessary to understand the assumptions that will be made to solve the degeneracy problem:

- Figure 7 shows the purity and the efficiency of the single hemisphere $b$ tag as a function of the purification cut $\delta = \Delta_b^{cut,high}$ . The purity and efficiency of the double hemisphere $b$ tag are also given, when the same $\Delta > \Delta_b^{cut,high}$ cut on $\Delta$ is applied to both sides. Without any $\Delta$ cut, the double tag purity is already 84% and approaches rapidly 100% when the cut is applied at the cost of a low efficiency. In practice, the $D_{66}$ component of the tensor with a cut on $\delta$ at 6 corresponds to almost pure $b$ events.

- The lego plot of fig. 8 shows for the simulation the population of the double tagged categories which is the input of the fit (the population for data shows the same features). The contributions of the three flavours are detailed also there. As can be seen *uds* and $b$ events populate opposite corners, while the $c$ events overlap largely with *uds* and $b$.

## 4.3 $\Gamma_{b\bar{b}}/\Gamma_{had}$ Measurement

An interesting feature of independent hemisphere tagging is that one can approach full $b$ purity in one hemisphere by imposing large values of the clear winning cut $\delta$ in the

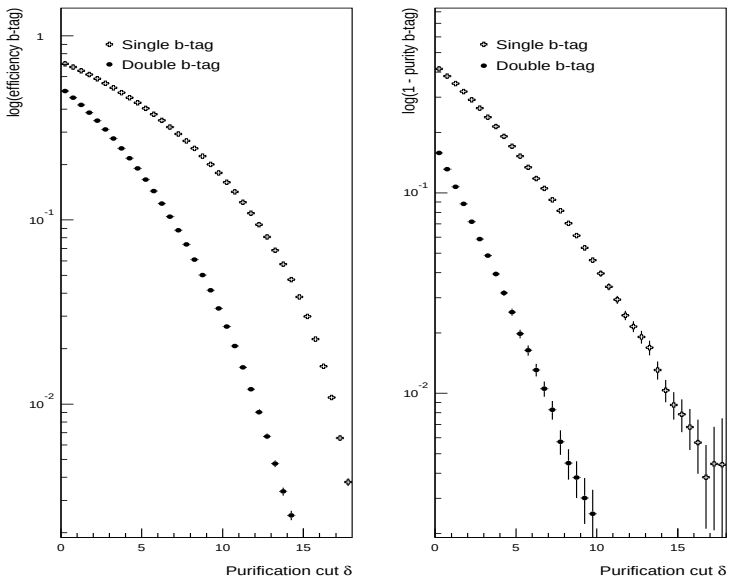


Figure 7: Efficiency and purity of the single and double hemisphere $b$ tags versus the value of the clear winning cut $\delta = \Delta_b^{cut}$ for simulated events.

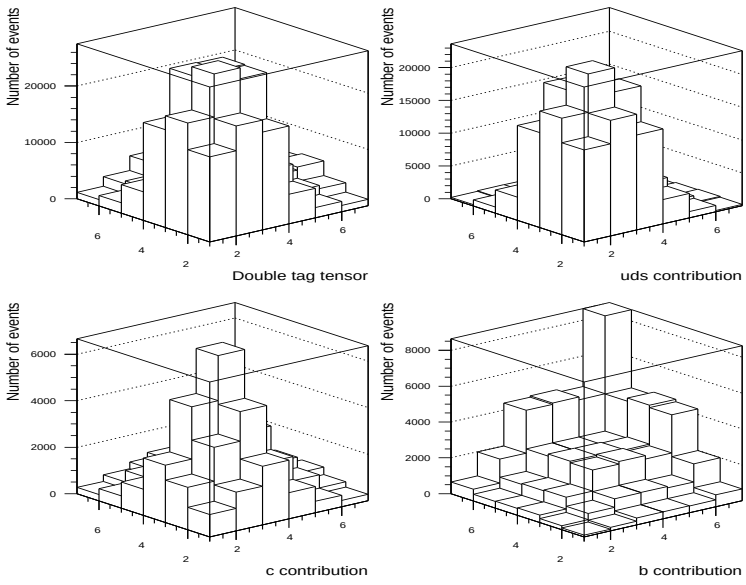


Figure 8: Population of the double-tag tensor with their uds, c and b contributions.

opposite one. This good separation achieved in the $b$ sector is not present in the other sectors.

Among the events which have been tagged as a $b$ in one hemisphere with a winning margin $\Delta > \delta$, consider the number, $N_I$, of events classified in the category $I$ for the other hemisphere and the fraction

$$f_I(\delta) = \frac{N_I(\delta)}{\sum_J N_J(\delta)} = \sum_l C_I^l R_l'(\delta) \tag{15}$$

where $R_l'(\delta)$ denotes the composition of the sample purified by the $\delta$ cut. When the clear winning cut, $\delta$, increases and if the hemispheres are independent, $f_I(\delta)$ tends to $C_I^b$. Formally

$$\lim_{\delta\to\infty} f_I(\delta) = C_I^b \tag{16}$$

since $R'_{uds}$, $R'_c$ and $R'_b$ tend to 0, 0 and 1 respectively, due to the fact that increasing $\delta$ results in samples with higher $b$ purity, as can be seen from fig. 6. It should be noted that in the eqn. 15 the contents of nearby bins are highly correlated. For this reason, in order to extract $C_I^b$ and to evaluate the statistical errors, we define the uncorrelated ratio $f_I^{uncorr}(\delta)$:

$$f_I^{uncorr}(\delta_i) = \frac{N_I(\delta_i) - N_I(\delta_{i+1})}{\sum_J [N_J(\delta_i) - N_J(\delta_{i+1})]} \tag{17}$$

which reaches the same limit as $f_I(\delta)$ for large values of $\delta$.

Different parameterizations of $f_I$ have been tried to fit the asymptotic value: uniform in the last bins of the distribution, exponential, inverse polynomial functions, etc. However, it was found experimentally that the best parameterization of our data is the exponential function

$$f_I(\delta) = p_1 \ + \ \frac{p_2}{\exp(p_3\delta + p_4\delta^3)} \tag{18}$$

where the $p_i$, $i = 1, ..., 4$ are free parameters of the fit. Only the parameter $p_1$ has physical meaning; it gives the asymptotic value. The plots of the $f_I^{uncorr}$ distributions for Monte Carlo and real data as a function of the clear winning cut value, $\delta$, are shown in figs. 9 and 10 respectively. For simulation, good agreement can be seen between the asymptotic limit and the expected $C_I^b$ matrix element. The validity of the asymptotic fit assumption, that there is no irreducible background from light and $c$ quarks, can be clearly seen in fig. 9.

Introducing the estimates $X_I^b$, we have minimized the function $G'(x, C)$ fixing the $R_c$ parameter to the measured value of $0.171 \pm 0.014$ [1]. As has already been remarked in section 4.1.2, fixing this parameter (to an arbitrary value) has no effect on any parameter of the $b$ sector. Table 5 compares the $C_I^b$ values obtained from the minimization with the $X_I^b$ estimates and with their expected values. Good agreement can be seen between the three sets of numbers. To some extent, the agreement between $C_I^b$ and $X_I^b$ is due to the fact that $X_I^b$ is used in the estimation of $C_I^b$. The fitted $b$ fraction for the simulated sample (after acceptance effects have been already considered) is found to be $R_b = 0.2174 \pm 0.0042$, to

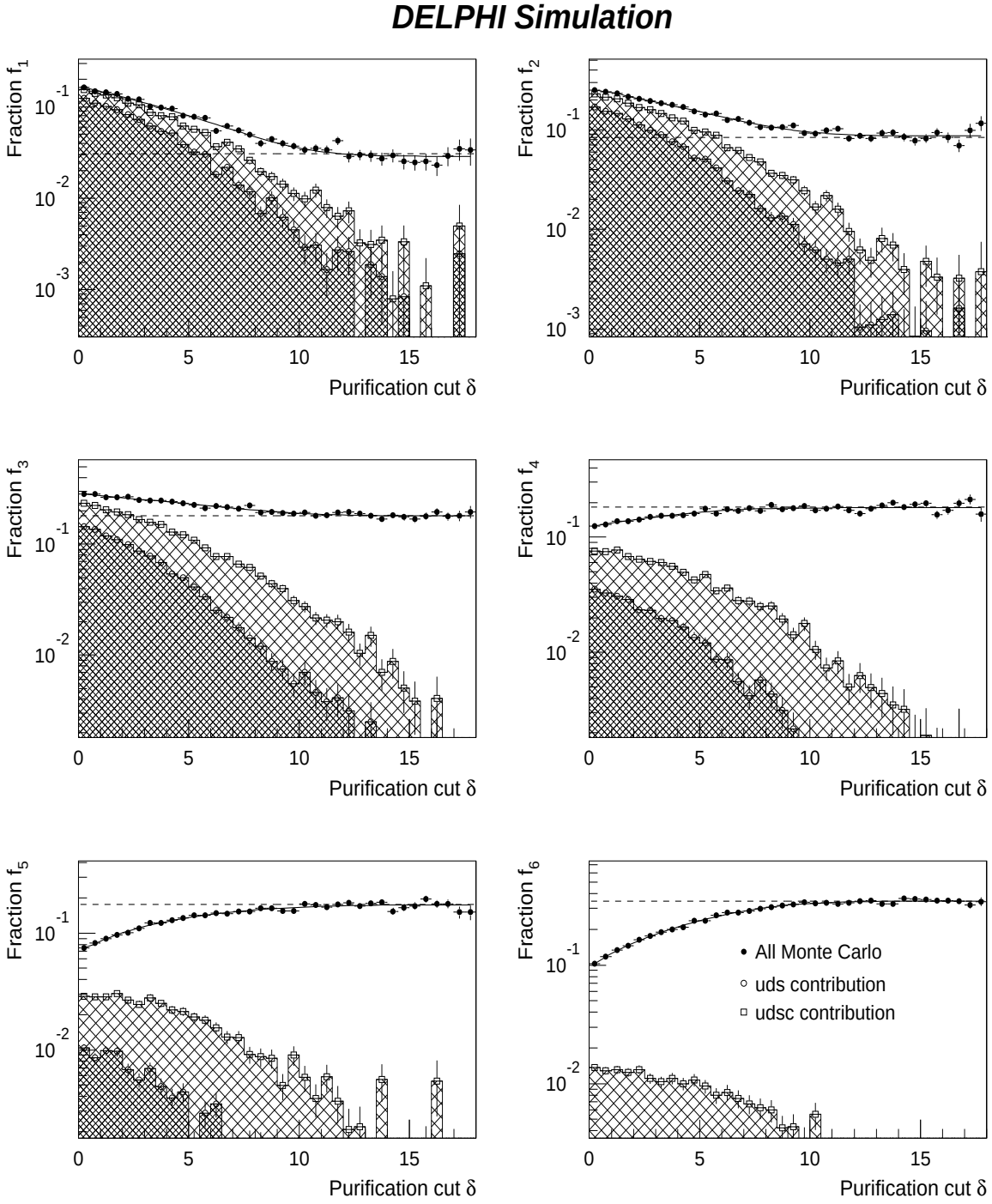


Figure 9: $f_I^{uncorr}(\delta)$ distributions with their asymptotic fits (see text) for Monte Carlo. If hemispheres are independent, $f_I^{uncorr}(\delta)$ should tend asymptotically to $C_I^b$ when $\delta$ increases. The big cross-hatched area indicates the $c$ contamination while the small cross-hatched area is the $uds$ contribution. No irreducible $uds$ and $c$ background is observed in the asymptotic region, specially in $f_4$, $f_5$ and $f_6$ distributions which are the most significant for the $R_b$ extraction. The dotted horizontal lines show the true values for $C_I^b$.

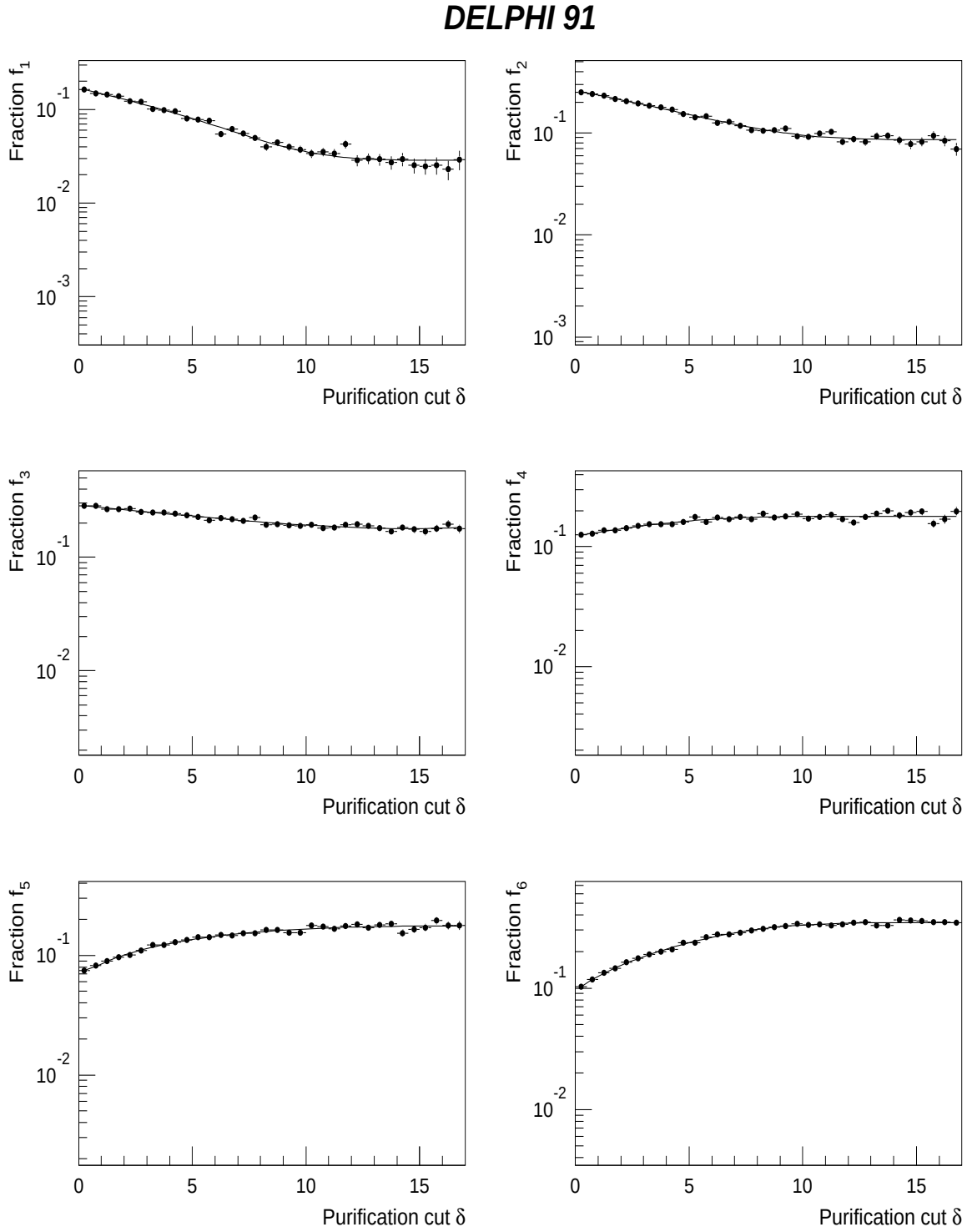


Figure 10: $f_I^{uncorr}(\delta)$ distributions with their asymptotic fits for DELPHI 91 real data.

| | *Simulated Data* | | | *Real Data* | |
|---|---|---|---|---|---|
| $C_I^b$ Matrix elements | *Expected values of* $C_I^b$ | *Asymptotic values* $X_I^b$ | *Fitted values of* $C_I^b$ | *Asymptotic values* $X_I^b$ | *Fitted values of* $C_I^b$ |
| $C_1^b$ | 0.0307 | 0.0290(20) | 0.0305(19) | 0.0294(23) | 0.0300(21) |
| $C_2^b$ | 0.0838 | 0.0853(29) | 0.0827(19) | 0.0634(33) | 0.0648(27) |
| $C_3^b$ | 0.1805 | 0.1768(55) | 0.1804(32) | 0.1486(43) | 0.1468(26) |
| $C_4^b$ | 0.1825 | 0.1800(30) | 0.1796(19) | 0.2126(28) | 0.2125(22) |
| $C_5^b$ | 0.1758 | 0.1744(41) | 0.1752(20) | 0.2026(43) | 0.2082(24) |
| $C_6^b$ | 0.3467 | 0.3489(45) | 0.3487(36) | 0.3393(71) | 0.3378(42) |

Table 5: $X_I^b$ parameters from asymptotic behaviour and the corresponding $C_I^b$ fitted values with the objective function $G'$, for simulated and real data sets. Comparison with the expected value for simulation. The errors are on the last two digits and are given in brackets.

be compared with the generated value of 0.217.

For the data, the values of $C_I^b$ are in agreement with the $X_I^b$s. After acceptance corrections the fitted $b$ fraction is

$$R_b = 0.2245 \pm 0.0063 \tag{19}$$

with $G'/ndf = 14.1/9$. The minimum of $G'(C,x)/ndf$ is very similar to that of the $G(C,x)/ndf$ function. This means that the $X_I^b$ introduced in the objective function are compatible with the set of degenerate solutions of the tensor fit alone. If another set of estimators $X_I^b$ is used the minimum of $G'(C,x)$ increases much more. For example, with the $X_I^b$ taken from Monte Carlo, $G'/ndf$ doubles.

## 4.4 Determination of Systematic Errors

The systematic errors have been determined separately for different sources. Only the most relevant ones are described in the following.

### 4.4.1 Hemisphere Correlation and $C^b$ Asymptotic Estimation

To allow for hemisphere correlations, the expressions for $T_{IJ}$ in the function $G'(C,x)$ are replaced by

$$T_{IJ} = \sum_l C_I^l C_J^l (1 + \rho_{JI}^l) R_l \tag{20}$$

where the double tag hemisphere correlation factor for a given flavour, $l$, is defined as

$$\rho_{JI}^l = \frac{D_{IJ}^l}{C_I^l C_J^l} - 1, \tag{21}$$

$D_{IJ}^l$ being the double tag efficiency. As before, the index $I$ refers to the first hemisphere tag and $J$ to the tag for the second. The correlation factors are predicted from the

simulation and are shown in fig. 11, with statistical errors, for the six categories. Most of these factors are small or not significant [4].

Correlations are also relevant for the asymptotic estimation of $C_I^b$, so that eqn. 16 is replaced by

$$\lim_{\delta\to\infty} f_I(\delta) = \left\{1 + \lim_{\delta\to\infty} \rho_{I6}^b(\delta)\right\} C_I^b \tag{22}$$

The main correlation factor for the $R_b$ measurement is $\rho_{66}^b$. Figure 12 shows the variation of this coefficient with $\delta$. It has no dramatic behaviour at large values of $\delta$ and for the standard cut is $\rho_{66}^b = 0.018 \pm 0.010$.

As a cross check, it is interesting to study how much $R_b$ changes when one uses eqns. 20 and 22 (where the $\lim_{\delta\to\infty} \rho_{I6}^b(\delta)$ have been approximated by $\rho_{I6}^b(6)$) assuming the hemisphere correlations shown in fig. 11 from the Monte Carlo, instead of eqns. 9 and 16. $R_b$ varies by less than 1 %.

In the absence of hemisphere correlations the $R_b$ measurement is in principle independent of the $b$ lifetime. However, in the presence of small correlations, the lifetime may change $R_b$. Therefore, we have checked whether the correlation depends on the $b$ lifetime, using the same simulated sample re-weighted to give different $b$ lifetimes (in order to minimize the statistical fluctuations). The change in $R_b$ was 0.0004 when $\tau_b$ changed from 1.6 ps to 1.2 ps. If one takes into account that the current uncertainty on the $b$ lifetime is 0.034 ps [8], this leads to a contribution smaller than 0.0001 on $R_b$.

The effect of hard gluon emission producing a $b\bar{b}$ pair in the same hemisphere (about 2 % of the $b\bar{b}$ events according to the simulation) might be the source of an excess of $b$ events in the $(small\ I, large\ J)$ and $(large\ I, small\ J)$ cells. However, the distributions of the tagging variables in "double $b$" hemispheres are, in the simulation, practically the same as in an ordinary $b$ hemisphere (the $B$ hadrons have a smaller energy, so that the $b$ character is not enhanced). This explains why there is no special accumulation of such hemispheres at large values of $\delta$, producing negative correlations in the $C_I^b$ estimates for large $I$ and corresponding positive one for low $I$. Actually we observe a small, but statistically significant depletion in the (1,6) bin of fig. 11. This suggests a cancellation with a correlation of opposite sign, maybe between the tagging variables. In order to evaluate systematic errors, we have performed a fits on the simulated data samples, removing the events with two $b$ jets in the same hemisphere and recomputing the $b$ fraction in the reduced sample. The difference between the fitted value of $R_b$ and the expected one is 0.0021. As in section 3.3, 20% of this number was taken as systematic uncertainty.

The stability of the asymptotic estimation of $C^b$ was tested using alternative $f_I$ parameterization functions, as described in 4.3. The $R_b$ values obtained by minimizing the $G'(C, x)$ objective function show a dispersion (for the different parameterizations used) of about 1 %.

The systematic error due to correlation effects (including contributions of the $C^b$ asymptotic estimation) was assumed to be well described in the simulation within the statistical error (0.0042), which can be taken, at this stage, as a conservative evaluation of the systematic error on $R_b$. Adding this error in quadrature to the uncertainty from hard gluon emission, the total systematic error does not change within the given accuracy. Moreover, we use the difference between fitted and expected $R_b$ on simulation (0.0004), as a correction to be applied to the $R_b$ fitted with the data.

[4] For example, the largest factor is $\rho_{11}^b = 0.52 \pm 0.15$, but it affects only 1/1000 of $b\bar{b}$ events.

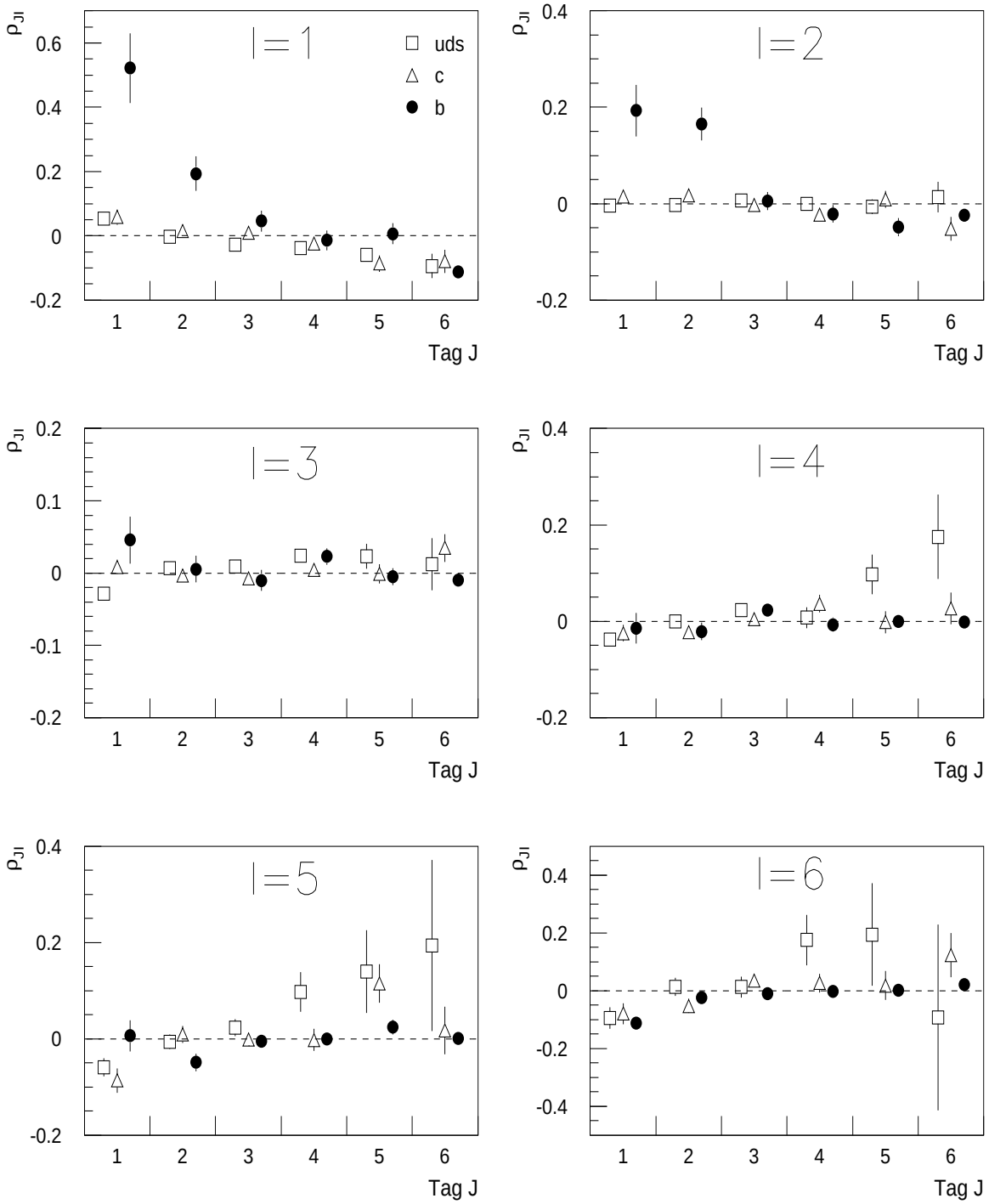


Figure 11: Double tag hemisphere correlation factors $\rho^l_{JI}$ for a given flavour, $l$.

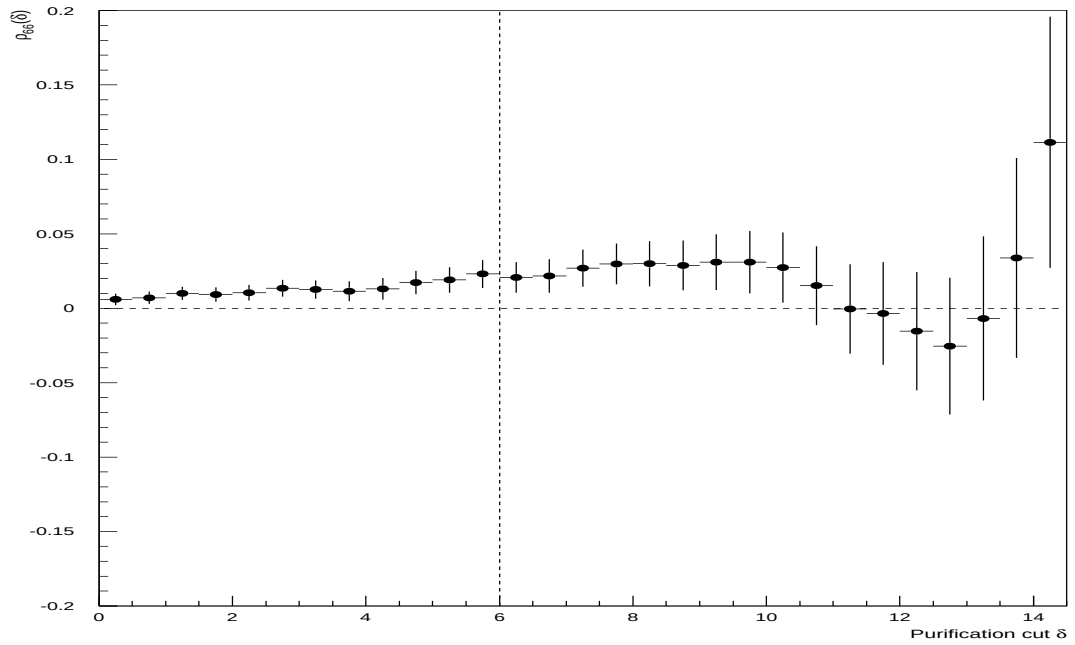


Figure 12: Double tag hemisphere correlation factor ($I = 6, J = 6$), as a function of $\delta$. For the standard cut at $\delta = 6$, the value of $\rho_{66}$ is $0.018 \pm 0.010$ and it remains rather stable over the whole range.

As a check on the correlation due to the limited VD acceptance, the cut on $\mid cos\theta_s \mid$ was moved from 0.65 to 0.85. No significant change was observed on $R_b$.

### 4.4.2 Effect of Tagging and Modelling

Two training samples have been used to compute the *"class-likelihoods"* of section 4.1 (with different lifetimes 1.2 and 1.6 ps, and different versions of the simulation program). We have found a difference of 0.0007 on $R_b$. Another effect to be considered is the choice of $\Delta_b^{cut,low}$ and $\Delta_b^{cut,high}$ which define the boundaries of $b$ categories. A change in the boundaries modifies the $C_4^b$, $C_5^b$ and $C_6^b$ values, but $C(b,b) = C_4^b + C_5^b + C_6^b$ and the compositions (in particular $R_b$) should remain constant. The spread of values gives a contribution to the systematic error of 0.0009. In principle the method is insensitive to tagging and modelling effects, but nevertheless we conservatively add these contributions.

### 4.4.3 Other Errors

- *Acceptance correction.* This contribution is mainly due to the selection criteria for hadronic Z events. The Monte Carlo is generated with a $\Gamma_{b\bar{b}}/\Gamma_{had}$ of 0.217. After acceptance cuts, this value is modified to $0.2211 \pm 0.0007$.

- *Dependence on* $\Gamma_{c\bar{c}}/\Gamma_{had}$. We refer here to actual number of charm events, which should be distinguished from $R_c$ in the fit. When changing the $c\bar{c}$ fraction by $\pm$ one

sigma of its measured value ($R_c = 0.171 \pm 0.014$ [1]), in the fit to the Monte Carlo we found a variation of 0.0012 $R_b$.

Table 6 summarizes the sources of systematic error and their contributions to the error on $\Gamma_{b\bar{b}}/\Gamma_{had}$.

Therefore we quote as final value, including acceptance and systematic corrections,

$$\Gamma_{b\bar{b}}/\Gamma_{had} = 0.2241 \pm 0.0063(stat.) \pm 0.0046(syst.). \quad (23)$$

# 5 Combination of the Methods

To combine the two measurements the statistical correlation has been measured by applying both methods to six independent Monte Carlo event samples yielding a correlation of 11% with large uncertainties. The corresponding 90% C.L. upper limit gives a correlation of 60%. Conservatively, this 60% correlation between the statistical errors has used in combining the two results.

The errors due to hemisphere correlation, $\Gamma_{c\bar{c}}$ and acceptance bias, have been taken as fully correlated between the two analyses; the rest were assumed to be uncorrelated. Table 6 summarizes the systematic errors of both analysis.

| Source of systematics | Significance Analysis | Multivariate Analysis |
|---|---|---|
| Hemisphere Correlation | 0.0031 | 0.0042 |
| $Br(Z \to b\bar{b})$ acceptance bias | 0.0010 | 0.0007 |
| Light quark efficiency | 0.0020 | |
| Charm efficiency | 0.0021 | |
| Effect of tagging and modelling | | 0.0011 |
| $\Gamma_{c\bar{c}}$ | 0.0019 | 0.0012 |
| Total | 0.0048 | 0.0046 |

Table 6: Systematic errors in the two analysis. Errors on the same line of the table (excluding the total) have been assumed to be fully correlated.

As our final result we find

$$R_b = 0.2209 \pm 0.0041\,(stat.) \pm 0.0042\,(syst.) \pm 0.0018\,(\Gamma_{c\bar{c}})$$

This value agrees well with the one measured by other experiments [3, 15] and with the one predicted by the Standard Model [2]. The current precision is not sufficient to constrain the Standard Model parameters. However with the analysis of the coming data, constraints on the top quark mass will be possible.

## Acknowledgements

We are greatly indebted to our technical collaborators and to the funding agencies for their support in building and operating the DELPHI detector, and to the members of the CERN-SL Division for the excellent performance of the LEP collider.

# References


[1] The LEP Collaborations, *Updated Parameters of the $Z^0$ Resonance from Combined Preliminary Data of the LEP Experiments*, CERN-PPE/93-157.

[2] W. Hollik, Fortsch.Phys. 38 (1990) 165.

[3] ALEPH collaboration, *A Precise measurement of* $\Gamma_{b\bar{b}}$ $/\Gamma_{had}$, CERN-PPE/93-108(1993).

[4] P. Aarnio *et al.* (DELPHI Collaboration). NIM A 303 (1991) 233-276.

[5] K.Hikasa *et al.* (Particle Data Group), Phys. Rev. **D45** (1992) n.11.

[6] D. Coffman *et al.* (MARK III Collaboration), Phys.Lett. **B263** (1991) 135.

[7] P.Abreu *et al.* (DELPHI Collaboration) Z.Phys. **C59** (1993) 533

[8] W. Venus *b Weak Interaction Physics in High Energy Experiments*, Talk given at *Cornell Conference*, 1993.

[9] D.Bardin *et al.*, *ZFITTER, An Analytical Program for Fermion Pair Production in* $e^+e^-$ *Annihilation*, CERN-TH 6443/92.

[10] P. Billoir et al., Measurement of the $\Gamma_{b\bar{b}}/\Gamma_{had}$ branching ratio of the $Z$ by hemisphere double tagging with minimal Monte Carlo dependence, Valencia pre-print in preparation.

[11] NAGLIB Manual. CERN Program Library.

[12] A.G. Frodesen, O. Skjeggestad, H. Tofte. 'Probability and Statistics in Particle Physics'. Universitetsforlaget 1979.

[13] Ch de la Vaissiere, S. Palma-Lopes. in the AIP Heavy Flavour workshop proceedings (1989) p440.

[14] P. Billoir *et al.* 'B-tagging by hemisphere: description of variables and results on Monte Carlo'. LPNHE pre-print in preparation.

[15] OPAL collaboration, R. Akers et al., CERN PPE 93–155;
L3 collaboration, O. Adriani et al. , Phys. Lett. 307B (1993) 237.